Scintillation properties and anomalous Ce^{3+} emission of $Cs_2NaREBr_6$: Ce^{3+} (RE=La,Y,Lu)

M. D. Birowosuto,* P. Dorenbos, and C. W. E. van Eijk

Radiation Detection and Matter, Faculty of Applied Sciences,

Delft University of Technology, Mekelweg 15, 2629 JB, Delft, The Netherlands

K. W. Krämer and H. U. Güdel

Department of Chemistry and Biochemistry,

University of Bern, Freiestrasse 3, 3000 Bern 9, Switzerland

(Dated: September 26, 2007)

Abstract

We report the optical and scintillation properties of the Ce^{3+} doped bromoelpasolites $Cs_2NaREBr_6$ (RE=La,Y,Lu). The γ-ray scintillation light yield of these materials varies from 6000 to 17.000 photons per MeV absorbed γ-ray energy. At room temperature (RT), the γ-ray scintillation decay curves for all compounds show a fast component of 61 ns, whereas the intrinsic Ce^{3+} decay time is 30 ns. The scintillation mechanism in elpasolites is addressed. In $Cs_2NaLuBr_6$: Ce^{3+} and Cs_2NaYBr_6: Ce^{3+}, we observe for the first time the so-called Ce^{3+} anomalous emission in bromide compounds. This emission previously observed for chloride compounds is an ultrafast Ce^{3+} emission with a selective excitation mechanism. The decay time of the anomalous emission at 10 K in bromide compounds ($\sim$7.80 ns) is faster than that in chloride compounds ($\sim$9.90 ns). Two bands of the anomalous emission are resolved for the first time. The mechanism behind this emission is discussed.

PACS numbers:

Keywords: elpasolites, spectroscopy, mechanism, anomalous emission.

*Electronic address: M. D. Birowosuto@tnw.tudelft.nl

I. INTRODUCTION

Elpasolites were thoroughly studied for applications such as laser hosts [1] and storage phosphors [2]. Recently, many Ce^{3+} doped elpasolites were investigated for inorganic scintillators, in particular for thermal neutron detection [3, 4, 5].

In Ce^{3+} doped elpasolites, Ce^{3+} ions occupy a high O_h symmetry site which splits the Ce^{3+} 5d levels into a lower triplet $5d_{t_{2g}}$ and an upper doublet $5d_{e_g}$. As in the case of the closely related perovskites, variants with lower symmetry occur, depending on composition, temperature or pressure. So far, elpasolites show less attractive scintillation properties than the lanthanum trihalides. The light yield in $LaBr_3$: Ce^{3+} is 70,000 photons/MeV, whereas that in Cs_2LiYBr_6: Ce^{3+} is 25,000 photons/MeV [6, 7]. The question why elpasolites show a lower light yield has remained open, due to lack of in-depth knowledge about the scintillation mechanism.

Van Loef *et al.* reported the influence of the anion on the scintillation mechanism of Ce^{3+} doped Cs_2LiYX_6 (X = Cl,Br)[4]. Van't Spijker *et al.* previously studied scintillation properties of Ce^{3+} doped $Cs_2NaRECl_6$ (RE=La,Lu)[8]. Optical and scintillation properties of Ce^{3+} doped $Cs_2NaREBr_6$ (RE=La,Y,Lu) are investigated in this work. The influences of the RE^{3+} ions on host properties and Ce^{3+} spectroscopy are discussed. Scintillation mechanisms, i.e. radiative transfer from a self trapped exciton (STE) to Ce^{3+}, STE migration, and binary vacancy (V_k) and electron diffusion, are addressed.

A so-called anomalous Ce^{3+} emission was observed recently in Cs_3LuCl_6: Ce^{3+}, Cs_2LiYCl_6: Ce^{3+} and $Cs_2LiLuCl_6$: Ce^{3+} [9, 10, 11]. The anomalous Ce^{3+} emission with a decay time of 10 ns is only observed when the $5d_e$ level is excited. It does not appear when the host lattice is excited. The application of this emission can be useful as a selective ultra-violet (UV) sensor. In the present paper, the same type of anomalous emission is observed for the first time in bromide compounds. Also for the first time, the emission shows clearly two bands that can be associated with the transitions to the $^2F_{5/2}$ and $^2F_{7/2}$ states of Ce^{3+}. The temperature dependence of the intensity and the decay times of the anomalous emission are presented, too.

II. EXPERIMENTAL TECHNIQUES

A. Crystal Growth

$Cs_2NaREBr_6$ (RE=La,Y,Lu) crystals were grown by the vertical Bridgman method using stoichiometric amounts of CsBr, NaBr and $REBr_3$ (RE = La, Y, Lu). $CeBr_3$ was used to prepare Ce^{3+}-doped compound. $Cs_2NaLaBr_6$: 0.5% Ce^{3+}, Cs_2NaYBr_6: 0.3% Ce^{3+} and $Cs_2NaLuBr_6$: 0.5% Ce^{3+} were grown. These cystals are hygroscopic and were sealed under argon atmosphere in small quartz ampoules to prevent hydration of the surfaces.

Cs_2NaYBr_6 and $Cs_2NaLuBr_6$ have the cubic elpasolite structure with four formula units in the unit cell (Cs_2NaYBr_6 with a = 11.30 Å; $Cs_2NaLuBr_6$ with a = 11.23 Å). $Cs_2NaLaBr_6$ is tetragonal (a = 11.52 Å and c = 11.61 Å) [12]. In $Cs_2NaLaBr_6$: Ce^{3+}, two La^{3+} sites can be occupied by Ce^{3+}. The space group of $Cs_2NaLaBr_6$ is P4/nbm (No. 125) and that of Cs_2NaYBr_6 and $Cs_2NaLuBr_6$ is $Fm\bar{3}m$ (No. 225).

B. Equipment

X-ray excited emission spectra were recorded using an X-ray tube with Cu anode operated at 35 kV and 25 mA. The emission was dispersed with an ARC VM504 monochromator, blazed at 300 nm with 1200 grooves mm^{-1}, and measured with a Hamamatsu R934-04 photomultiplier tube (PMT). The spectra were corrected for the transmittance of the monochromator and the quantum efficiency of the PMT.

Time resolved excitation and emission spectra with high resolution at temperatures between 10 and 300 K were recorded at the SUPERLUMI vacuum ultraviolet (VUV) station of Hamburger Synchrotronstrahlungslabor (HASYLAB) at the Deutsches Elektronen-Synchrotron (DESY) facility in Hamburg, Germany. Emission spectra were recorded with an ARC Spectropro 300I monochromator, blazed at 500 nm with 300 grooves mm^{-1}, and a R6358 Hamamatsu PMT. Excitation spectra were recorded using a 0.3 nm resolution McPherson monochromator with a working range of 50-330 nm. Photons were counted within a time window of 20 ns, 6 ns after following the start of the excitation synchrotron pulse. Another 65 ns wide time window starting after 85 ns delay was used to discriminate between fast and slow luminescence components. Integral spectra comprising all emitted light were also recorded. With the same setup, we recorded decay time curves. Details about

the SUPERLUMI station were published by Zimmerer [13]. Ultra violet/visible (UV/VIS) excitation and emission spectra measured at RT with an observation of wavelengths longer than 330 nm were performed with a spectrophotometer type Quanta Master QM1 of Photon Technology International.

Pulse height spectra under γ-ray excitation from a ^{137}Cs source were recorded with a Hamamatsu R1791 PMT with a box type dynode structure connected to a pre-amplifier and an Ortec 672 spectroscopy amplifier. The quartz ampoules containing the crystals were optically coupled onto the PMT window with Viscasil 60 000 cSt from General Electric. The quartz ampoules were covered with several layers of 0.1 mm UV reflecting Teflon tape for better light collection. The yield expressed as photoelectrons per MeV (phe/MeV) of absorbed γ-ray energy, was obtained by comparison of the peak position of the 662 keV photopeak in the pulse height spectra with the peak position of single photoelectron response. The light yield expressed in photons/MeV is determined by correcting for the quantum efficiency and the reflectivity of the PMT [14].

Scintillation decay time curves under ^{137}Cs 662 keV γ-ray excitation were recorded with the multi-hit method. A description about the experimental setup can be found elsewhere [15, 16]

III. RESULTS

A. X-ray excited emission spectra

X-ray excited emission spectra of Ce^{3+} doped $Cs_2NaREBr_6$ (RE=La,Y,Lu) are shown in Figure 1. The maximal intensity for each spectrum has been normalized and vertically shifted with respect to each other for clarity.

Characteristic 5d→4f $Ce^{3+}[^2F_{5/2}, ^2F_{7/2}]$ doublet emission is well resolved in the spectra. The 5d→$^2F_{5/2}$ emission is peaked at 382, 385, and 389 nm for $Cs_2NaLaBr_6$: Ce^{3+}, Cs_2NaYBr_6: Ce^{3+} and $Cs_2NaLuBr_6$: Ce^{3+}, respectively. The 5d→$^2F_{7/2}$ emission is peaked at 414, 420, and 422 nm for $Cs_2NaLaBr_6$: Ce^{3+}, Cs_2NaYBr_6: Ce^{3+} and $Cs_2NaLuBr_6$: Ce^{3+}, respectively. In X-ray excited emission spectra of Cs_2LiYCl_6: Ce^{3+}, $Cs_2LiLuCl_6$: Ce^{3+} and Cs_2LiYBr_6: Ce^{3+}, an additional low intensity emission band was observed at shorter wavelength [4, 10, 11]. This band was attributed to a remnant of STE emission.

We do not observe such band in the X-ray excited emission spectra of $Cs_2NaREBr_6$: Ce^{3+} (RE=La,Y,Lu) recorded at RT, see Figure 1.

B. Gamma spectroscopy

The ^{137}Cs 662 keV γ-ray pulse height spectra of Ce^{3+} doped $Cs_2NaREBr_6$ (RE=La,Y,Lu) are presented in Figure 2. Light yields derived from the pulse height spectra are compiled in Table I. $Cs_2NaLaBr_6$: Ce^{3+} has the highest light yield of 17,000 photons/MeV. The yield decreases when RE^{3+} changes from La^{3+} to Y^{3+} to Lu^{3+}. Such a decrease was not observed for Ce^{3+} doped $Cs_2NaRECl_6$ (RE=La,Lu) but it was observed for $Cs_2LiRECl_6$: Ce^{3+} (RE=La,Y,Lu) [3, 7, 8, 11]. The contribution of the fast components (within 0.5 μs shaping time) to the total light yield of $Cs_2NaLaBr_6$: Ce^{3+},Cs_2NaYBr_6: Ce^{3+} and $Cs_2NaLuBr_6$: Ce^{3+} is 53, 53 and 90 %, respectively. The energy resolutions of these materials are still far from the best energy resolution of 2.8 % recorded for $LaBr_3$: Ce^{3+}, see column 5 in Table I [6].

C. Scintillation and intrinsic Ce^{3+} emission decay times

Figure 3 shows scintillation and optical excited Ce^{3+} emission decay curves of Ce^{3+} doped $Cs_2NaREBr_6$ (RE=La,Y,Lu). The scintillation decay curves were recorded at RT, whereas the Ce^{3+} emission decay curves were recorded at 10 K and RT. The Ce^{3+} emission decay curves of $Cs_2NaLaBr_6$: Ce^{3+} were excited at 330 nm and the emission monitored at 384 nm, whereas those of Cs_2NaYBr_6: Ce^{3+} and $Cs_2NaLuBr_6$: Ce^{3+} were excited at 328 nm and the emission monitored at 380 nm.

The scintillation decay curves are characterized by three decay components; a fast, an intermediate and a slow component. In Table II, the three decay components are presented as well as their relative contribution to the total light output of the crystals. Intrinsic decay times of the Ce^{3+} emission at 10 K and RT are also presented. They are obtained from single exponential fits of the decay curves after excitation of the $5d_t$ state.

The fast component of the scintillation decay remains 61 ns when changing the cation from La^{3+} to Y^{3+} to Lu^{3+} but there are differences for the intermediate and slow components. The optically excited spectra at 10 K exhibit the same 24 ns Ce^{3+} emission decay time, see

inset in Figure 3. At RT, these decay times increase to 30 ns. A similar decay time increase with temperature is reported for Ce^{3+} emission in other compounds [17].

D. Spectroscopy

The optically excited emission spectra of Ce^{3+} doped $Cs_2NaREBr_6$ (RE=La,Y,Lu) at 10 K are shown in Figure 4. The spectra were normalized to each other in order to demonstrate best the different contributions. Slow(i) and fast(ii) emission spectra were excited into the host lattice absorption and the Ce^{3+} 4f→5d$_e$ bands, and are shown as dotted and full lines, respectively, in Figure 4(a-c).

The fast emission spectra excited into the Ce^{3+} 4f→5d$_e$ band exhibit two bands of the characteristic 5d→4f Ce^{3+} doublet emission around 400 nm. The ^2F spin orbit splittings of the Ce^{3+} ground state in $Cs_2NaLaBr_6$: Ce^{3+}, Cs_2NaYBr_6: Ce^{3+}, and $Cs_2NaLuBr_6$: Ce^{3+} are 2023, 2165, and 2010 cm^{-1} (0.25, 0.27, and 0.25 eV), respectively. Two other fast doublet emissions with maxima at 282 and 285 nm are observed for Cs_2NaYBr_6: Ce^{3+} and $Cs_2NaLuBr_6$: Ce^{3+}, respectively. Similar high energy emissions under excitation in 5d$_e$ were previously observed in the chloride compounds Cs_3LuCl_6: Ce^{3+}, Cs_2LiYCl_6: Ce^{3+}, and $Cs_2LiLuCl_6$: Ce^{3+} [9, 10, 11], where they were called anomalous Ce^{3+} emissions. For the bromoelpasolites in Figure 4, we observe a clear doublet structure of this emission that was not observed before. The doublets are separated by 2055 and 2022 cm $^{-1}$ (0.25 and 0.25 eV) for Cs_2NaYBr_6: Ce^{3+} and $Cs_2NaLuBr_6$: Ce^{3+}, respectively. Considering of an error of 10 %, these energy differences correspond to the spin orbit splittings between ^2F states.

Beside the normal and anomalous Ce^{3+} emission, the slow emission spectra excited into the host lattice absorptions show emissions at 345 and 325 nm for Cs_2NaYBr_6: Ce^{3+} and $Cs_2NaLuBr_6$: Ce^{3+}, respectively. These emissions are attributed to a remnant of STE emission. Such emissions were often observed in other elpasolites [9, 10, 11].

The excitation spectra of the STE emission remnants at 360, 345, and 325 nm for $Cs_2NaLaBr_6$, Cs_2NaYBr_6 and $Cs_2NaLuBr_6$, respectively, are shown as curves (ii) in Figure 5(a-c). From those spectra, properties of the host compounds which are compiled in Table III were derived. The fundamental absorption (E^{fa}) is the energy of the first sharp onset in the slow excitation spectra of the STE emission. The first maximum (E^{ex}) is attributed to the creation of excitons which can be regarded as bound electron hole pairs. The

edge of the conduction band (E_{VC}) corresponds to the creation of free electrons in the conduction band and free holes in the valence band. We estimate the bottom of the conduction band at 8% higher energy than E^{ex}.

The integral excitation spectra of the 5d→4f Ce^{3+} emission recorded at RT show the Ce^{3+} 4f→5d excitation bands. For elpasolites, we expect the $5d_t$ levels at lower energy and the $5d_e$ levels at higher energy due to the octahedral crystal field splitting. Most of the 4f→5d bands overlap. The level positions were determined by fitting multiple Gaussians to the $5d_e$ and the $5d_t$ bands. In the excitation spectrum of $Cs_2NaLuBr_6$: Ce^{3+}, see Figures 5c(i), a splitting of the $5d_e$ levels is observed. We refer to the high energy band at 226 nm as $5d_{e2}$ and to the low energy one at 235 nm as $5d_{e1}$. The fitted energies of the 5d levels of Ce^{3+} are compiled in Table IV. We observed another fast excitation band at 212 nm for $Cs_2NaLuBr_6$: Ce^{3+}. This band is not attributed to Ce^{3+} 4f→5d excitation.

The fast excitation spectra at 10 K monitoring the anomalous emission of Cs_2NaYBr_6: Ce^{3+} and $Cs_2NaLuBr_6$: Ce^{3+} show a Ce^{3+} 4f→$5d_e$ excitation band, see Figure 5b(iii) and c(iii). The Ce^{3+} 4f→$5d_{e1}$ excitation band is shifted from 233 and 235 nm at RT to 226 nm at 10 K for $Cs_2NaLuBr_6$: Ce^{3+} and Cs_2NaYBr_6: Ce^{3+}, respectively. This anomalous excitation band has a cut off on the short wavelength side. If we excite at the 4f→$5d_{e2}$ Ce^{3+} band, it does not lead to the anomalous emission. The anomalous emission is also absent in the X-ray excited emission spectra, see Figure 1. It means that there is no energy transfer from the host lattice to the anomalous emitting state.

Besides 4f→5d Ce^{3+} and host lattice excitation bands, we observed some other bands. Two bands at 217 and 222 nm for $Cs_2NaLuBr_6$: Ce^{3+} and Cs_2NaYBr_6: Ce^{3+}, respectively, are tentatively assigned to a kind of near defect exciton (NDE), see Figure 5b(ii) and c(ii). NDEs are excitons created in the near vicinity of an impurity. We also observed three fast bands at 262, 279 and 295 nm in the excitation spectrum of $Cs_2NaLaBr_6$: Ce^{3+}, see Figure 5a(iii). Although they are fast and connected to Ce^{3+} emission, the origin of these bands is not clear.

E. Temperature Dependence of Anomalous Emission

Figure 6 shows the emission spectra of $Cs_2NaLuBr_6$: Ce^{3+} excited into the 4f→$5d_{e1}$ Ce^{3+} band (226 nm) and their integrals as a function of temperature. With increasing

temperature, the anomalous emission quenches and fully disappears at 110 K. At the same time, the $5d_t \rightarrow 4f$ Ce^{3+} emission increases.

Figure 7a shows the decay time curves of the anomalous emission at 282 nm excited in the $4f \rightarrow 5d_{e1}$ band of $Cs_2NaLuBr_6$: Ce^{3+} at 226 nm as function of temperature. All spectra show a single exponential decay. The decay time of 7.83 ns is constant up to about 60 K, see Figure 7b. It drops at higher temperature. The temperature at which the decay time of the anomalous emission decreases more or less corresponds to the temperature where the anomalous emission intensity decreases and the Ce^{3+} $5d_t \rightarrow 4f$ emission intensity increases, see Figure 6. This anticorrelation between anomalous emission and Ce^{3+} $5d_t \rightarrow 4f$ emission was also observed for Cs_3LuCl_6: Ce^{3+}, Cs_2LiYCl_6: Ce^{3+}, and $Cs_2LiLuCl_6$: Ce^{3+}[9, 10, 11].

The dotted line through the data in Figure 7b is a fit by Equation 1 used to describe the thermal luminescence quenching. The decay time of anomalous emission (τ_a^q) is calculated as [10]

$$\tau_a^q(T) = \frac{1}{\frac{1}{\tau_a} + \Gamma_0 \exp(\frac{-\Delta E_q}{kT})} \tag{1}$$

where τ_a is the 7.83 ns radiative decay time of anomalous emission assumed to be temperature independent. Γ_0 is the thermal quenching rate at T = ∞ K (attempt rate), ΔE_q is the activation energy for thermal quenching, and k is the Boltzmann constant. A fit to Equation 1 yields values of $\Gamma_0 = 3.21\ 10^{12}$ Hz and $\Delta E_q = 0.08$ eV.

The decay curves of the Ce^{3+} $5d_t \rightarrow 4f$ emission at 385 nm in $Cs_2NaLuBr_6$: Ce^{3+} into the $4f \rightarrow 5d_{e1}$ excited at 226 nm, are shown in Figure 8 on a linear scale. The spectra in Figure 8 show different features than those of the anomalous emission in Figure 7.

The decay time becomes slower when the temperature increases, see Figure 8. Between 50 and 110 K, the curves show a slow rise time in the first 3-10 ns leading to a delayed $5d_t \rightarrow 4f$ emission. The delay is most prominent at 90 K. For higher temperatures, the rise time becomes faster and the decay tends to return to single exponential with a decay time close to that of the Ce^{3+} $5d_t \rightarrow 4f$ emission under direct $4f \rightarrow 5d_t$ excitation.

The inset in Figure 8 shows the decay time τ_d of the Ce^{3+} emission upon $4f \rightarrow 5d_t$ excitation at 333 nm as a function of temperature. The corresponding decay time curve at 10 K was already shown as inset in Figure 3. Some values are also listed in Table VI. τ_d increases from 24.0 ns at 10 K to 25.3 ns at 110 K.

IV. DISCUSSION

A. Host properties

Table III compiles the host properties E^{fa}, E^{ex} and E_{VC} of $Cs_2NaREBr_6$ (RE=La,Y,Lu). The tabulated energies increase in the series La^{3+} to Y^{3+} to Lu^{3+}. We expect that the bottom of the conduction band is formed by the lanthanide orbitals. The ionic radius of La^{3+} is 13 pm larger than that of Y^{3+} and 17 pm larger than that of Lu^{3+} leading to larger La^{3+}-Br^{-} distances, see Table IV [18]. The negative Madelung potential at RE^{3+} site increases with smaller RE^{3+} size resulting the increase of the tabulated energies in Table III.

B. Ce^{3+} spectroscopy

The energy to excite a Ce^{3+} from its 4f ground state to the lowest energy 5d state in a free ion is 51 230 cm^{-1}. When Ce^{3+} ions are placed in a crystalline environment, this energy becomes smaller. It is determined by (i) the crystal field splitting ϵ_{cfs} of the 5d configuration and (ii) the centroid shift ϵ_c [19]. The spectroscopic and crystallographic properties of Ce^{3+} doped $Cs_2NaREBr_6$ (RE=La,Y,Lu) are shown in Table IV.

The crystal field splitting is controlled by the size and shape of the bromide ion polyhedron coordinating the Ce^{3+} ion. The size of the polyhedron is approximated by the average distance R_{av} of the cation to the N coordinating anions with a correction of $0.6\Delta R$ accounting for lattice relaxation [20]. ΔR is defined as the difference in ionic radius between Ce^{3+} and the cation it substitutes for. It amounts to 2, -11, and -15 pm for La^{3+}, Y^{3+}, and Lu^{3+}, respectively. ϵ_{cfs} is empirically modelled by Equation 2 [20]:

$$\epsilon_{cfs} = \beta_{poly}(\frac{1}{N}\sum_{i=1}^{N}(R_i - 0.6\Delta R))^{-2} \quad (2)$$

where β_{poly} is a constant that depends on the type of coordination polyhedron. Figure 9 shows the crystal field splitting data of some elpasolites. The dotted curve through the data is a fit to Equation 2. From this fit, we obtained $\beta_{elpasolite} = 1.33 \times 10^9$ pm^2cm^{-1}. It corresponds well with β values of compounds with octahedral coordination (1.35×10^9 pm^2cm^{-1}) reported previously by Dorenbos [21].

In Table IV, ϵ_{cfs} increases in the sequence La^{3+} to Y^{3+} to Lu^{3+}. A similar trend is also observed for $Cs_2NaRECl_6$: Ce^{3+} (RE=La,Y,Lu), see Figure 9. It shows that the smaller

the cation site occupied by Ce^{3+} is the larger is ϵ_{cfs}. A larger ϵ_{cfs} shifts the Ce^{3+} emission towards longer wavelengths, see Figures 1 and 4.

The centroid shift is the lowering of the average position (barycenter) of the 5d levels of Ce^{3+} in a host crystal. From Table IV, ϵ_c decreases in the sequence La^{3+} to Y^{3+} to Lu^{3+} by about 400 cm^{-1} as a result of increasing 5d-ligand covalency. Compared to the increase of the crystal field splitting in the sequence La^{3+} to Y^{3+} to Lu^{3+}, this decrease has a smaller influence on the energy of the Ce^{3+} 4f→5d transition.

The Stokes shift in the bromoelpasolites is smaller than that in the chloroelpasolites, see column 8 in Table IV and ∼0.18 eV for Cs_2LiYCl_6: Ce^{3+} and $Cs_2LiLuCl_6$: Ce^{3+}[4, 11]. It is caused by the shorter bond length shifts as a consequence of a smaller vibrational frequency in the bromoelpasolites than in the chloroelpasolites [23].

C. Scintillation mechanism

Scintillation mechanisms in elpasolites crystals were previously discussed by Dorenbos [24]. Different energy transfer mechanisms to Ce^{3+} occur at different timescales and with different probabilities. Radiative transfer through re-absorption of STE emission by Ce^{3+}, STE migration, and binary V_k center and electron diffusion are possible mechanisms. It was suggested that an energy transfer by direct electron-hole capture does not occur in elpasolites. For direct capture, one would expect a decay component of 30 ns, similar to the decay for optical excitation of the 5d state at RT. However, the fast decay component for γ-excitation is 61 ns for all the elpasolites, see Table II. This implies that there is a delayed transfer to Ce^{3+} that does not depend on the type of RE^{3+} ions.

For Ce^{3+} doped $Cs_2NaREBr_6$ (RE=La,Y,Lu), the radiative energy transfer from STE to Ce^{3+} is not an important excitation mechanism because of the absence of the STE emission in the X-ray excited emission spectra, see Figure 1.

Additional mechanisms might be the non-radiative energy transfers from STE to Ce^{3+}, i.e. *STE diffusion*, or *the binary electron-hole recombination on* Ce^{3+}. In the first case, the transfer rate from STE to Ce^{3+} increases with temperature and results in an increased Ce^{3+} luminescence on the expense of STE luminescence [25]. In the second case, after the creation of an STE, the bound electron and hole separate again and form an F-H and F-V_k pair [26]. For rising temperature, the number of loosely bound electrons (F centers) and

holes (H or V_k center) increases. At a certain temperature, they start to migrate through the lattice and a V_k center can be trapped or stabilized near a Ce^{3+} ion. The recombination with an electron will excite Ce^{3+}. It is also possible that first the electron is trapped by Ce^{3+} and subsequently, the V_k diffuses and recombines with the (Ce^{3+}-e^-) center to yield Ce^{3+} luminescence. We propose that *this binary-electron hole recombination on Ce^{3+}* plays the important role in energy transfer.

D. Anomalous Emission

Figure 10 shows a configuration coordinate diagram for anomalous emission in $Cs_2NaLuBr_6$: Ce^{3+}. A very similar diagram was used to explain anomalous emission in Cs_3LuCl_6: Ce^{3+} [9] and later in Cs_2LiYCl_6: Ce^{3+} [10] and $Cs_2LiLuCl_6$: Ce^{3+} [11]. The anomalous emission is only observed when an electron is excited from the 4f ground state to the $5d_{e1}$ or small part of the $5d_{e2}$ levels. In the following discussion, we only consider the mechanism involving the $5d_{e1}$ excitation with the assumption that the mechanism for the $5d_{e2}$ excitation is the same.

Arrow 1 in Figure 10 symbolizes the 4f→$5d_t$ excitation. It leads to the normal doublet $5d_t$ →4f $Ce^{3+}[^2F_{5/2},^2F_{7/2}]$ emission symbolized by arrow 2. For this emission, a decay time of 24 ns was recorded at 10 K, see Figure 3. The 4f→$5d_{e1}$ excitation indicated by arrow 3 can be followed by different steps. The $5d_{e1}$ state may decay through multi-phonon relaxation to the $5d_t$ states followed by normal $5d_t$ →4f emission (arrow 2). This relaxation is not likely for chloroelpasolites due to a large energy gap of 2.07-2.50 eV between the $5d_{e1}$ and $5d_t$ states and the small maximum phonon frequency [9, 11]. In $Cs_2NaLuBr_6$: Ce^{3+}, the energy gap of 1.65 eV between the $5d_{e1}$ and $5d_t$ states is smaller than in $Cs_2LiLuCl_6$: Ce^{3+} and Cs_3LuCl_6: Ce^{3+}. However, the multi-phonon relaxation in $Cs_2NaLuBr_6$: Ce^{3+} is still not favorable due to the smaller maximum photon frequency. Instead the following return transition from $5d_{e1}$ to Ce^{3+} was proposed [9, 10, 11].

An electron in the $5d_{e1}$ state auto-ionizes to the conduction band indicated by arrow 4. This electron, somehow, remains localized in the attractive Coulomb potential of the Ce^{4+} ion left behind. The electron relaxes to the ground state of this anomalous state located below the conduction band by an amount similar to the binding energy of the electron to Ce^{4+}. We predict that this energy has the same order as the exciton binding energy (0.5

eV). The radiative recombination of the electron in the anomalous state with the hole left behind on Ce^{4+} leads to the fast 0.81 eV Stokes shifted emission at 265 nm indicated by arrow 5. The doublet splitting of the anomalous emission of 0.25 eV is consistent with the 0.25 eV splitting between $^2F_{5/2}$ and $^2F_{7/2}$ states of Ce^{3+}. This splitting was not previously observed for chloride compounds. In order to further analyze this splitting, the widths of the Ce^{3+} emission bands (full width at half maximum (FWHM)) in chloroelpasolites and bromoelpasolites are compiled in Table V.

From Table V, we observe that the ordinary Ce^{3+} emission bands in bromoelpasolites are narrower than in chloroelpasolites. The difference is larger for the $5d \rightarrow {}^2F_{7/2}$ Ce^{3+} emission. The narrower emission band is attributed to the smaller breathing mode vibrational frequencies in bromoelpasolites ($\sim$200 cm^{-1}) than in chloroelpasolites ($\sim$300 cm^{-1}) [23]. This is also related with the anomalous Ce^{3+} emission. Thus, the splitting of the anomalous emission is resolved in bromoelpasolites but not in chloroelpasolites.

In Figure 6, the anomalous emission intensity decreases with increasing temperature which is accompanied by an increase of the $5d_t \rightarrow 4f$ emission. This is explained by a temperature activated energy transfer from the anomalous state to the $5d_t$ emitting state symbolized by arrow 6 in Figure 10. The thermal activation energy of 0.08 eV calculated for this process, see Equation 1, is attributed to the energy difference between the bottom of the anomalous state and the crossing point in the configurational coordinate diagram with the parabola of the $5d_t$ in Figure 10.

This whole energy transfer mechanism was modelled by a set of rate equations in References [9, 10, 11]. Here we will use the same model. $N_a(t)$ is the number of populated anomalous states that has a rate $\Gamma_a(T)$ for decreasing radiatively by anomalous emission and a rate $\Gamma_t(T)$ for decreasing by transfer to the $5d_t$ state due to thermal activation. The change in $N_a(t)$ is given by

$$\frac{dN_a(t)}{dt} = -\Gamma_a(T)N_a(t) - \Gamma_t(T)N_a(t) \tag{3}$$

$N_d(t)$ is the number of populated $5d_t$ states with a rate $\Gamma_d(T)$ for decreasing by radiative transitions to the 4f ground state. The time derivative of $N_d(t)$ is given by

$$\frac{dN_d(t)}{dt} = -\Gamma_d(T)N_d(t) + \Gamma_t(T)N_a(t) \tag{4}$$

From both equations, the solutions are given by

$$N_a(t) = N_a(0)e^{-(\Gamma_a(T)+\Gamma_t(T))t} \tag{5}$$

and

$$N_d(t) = N_d(0)e^{-\Gamma_d(T)t} + \frac{\Gamma_t(T)N_a(0)}{\Gamma_a(T)+\Gamma_t(T)-\Gamma_d(T)} \times(e^{-\Gamma_d(T)t} - e^{-(\Gamma_a(T)+\Gamma_t(T))t}) \tag{6}$$

where $N_a(0)$ and $N_d(0)$ are the initial population at t=0 of the anomalous and $5d_t$ states, respectively. $\Gamma_d(T) = 1/\tau_d$ is known from experiment, see Figure 8b, and compiled in Table VI. $\Gamma_a(T) + \Gamma_t(T)$ and $\Gamma_t(T)N_a(0)$ are treated as the unknown parameters of Equation 6.

Figure 11 shows the decay curves of Ce^{3+} $5d_t \rightarrow 4f$ emission excited in the $5d_{e1}$ state and in the $5d_t$ state for 60, 90, and 110 K. Curves excited in the $5d_t$ state are normalized to 1 at time $t = 0$, and are fitted with a single exponential with the decay times $\tau_d(T)$ listed in Table VI. The curves excited in the $5d_{e1}$ level were modelled using Equation 6 with the same $\Gamma_d(T)$ values and $N_d(0) = 1$. Values for $\tau_a^{tot} = 1/(\Gamma_a+\Gamma_t)$ and $1/\Gamma_t$ in columns 3 and 4 in Table VI were calculated with the Γ_0 and ΔE_q parameter of Equation 1. The values obtained from the fit for $1/(\Gamma_a+\Gamma_t)$ and $\Gamma_t N_a(0)/N_d(0)$ are compiled in columns 5 and 6 of Table VI, respectively. The model yields a good simulation for the observed decay curves.

For temperature above 60 K column 3 agrees satisfactorily with column 5. This is the proof that the anomalous emission is quenched by means of energy transfer to the $5d_t$ state of Ce^{3+}. There are disagreements for temperatures below 60 K. The values are larger than 7.83 ns, see column 5 in Table VI. Presumably, besides excitation of the $5d_{e1}$ state, also other centers are excited at 226 nm that may transfer energy to Ce^{3+}[11]. Multiplying column 4 with column 6 in Table VI provides $N_a(0)/N_d(0)$ in column 7. The larger values at lower temperatures suggest that upon excitation of the $5d_{e1}$ state, the relaxation to the anomalous state at low temperature is more probable than to the $5d_t$ state.

We compare the quenching parameters for Cs_2NaYBr_6: Ce^{3+} and $Cs_2NaLuBr_6$: Ce^{3+} with those of the previously studied chloride compounds in Table VII. The decay time of the anomalous emission (τ_a) in the bromoelpasolites ($\sim$7.80 ns) is faster than that in chloride compounds ($\sim$9.90 ns), see column 2 in Table VII. The average anomalous emission wavelength ($\overline{\lambda}_{an}$) ranges from 267 to 281 nm. For the following discussion, the relation between

the decay time τ and the emission wavelength λ of an electric dipole allowed transition is given by [27, 28]

$$\frac{1}{\tau} \propto \frac{n}{\lambda^3}(\frac{n^2+2}{3})^2 \sum_f | < f|\mu|i > |^2 \quad (7)$$

where n is the refractive index. The summation over the matrix elements connecting an initial state $|i >$ with a final state $|f >$ via the dipole operator μ gives the oscillator strength [28].

The ratio of τ/λ^3 between the anomalous Ce^{3+} emission and the ordinary Ce^{3+} emission is close to unity, see column 5 in Table VII. This means that the anomalous Ce^{3+} emission is an electric dipole allowed transition. The slightly lower values than unity can be related with the difference between the oscillator strength of the anomalous and that of the ordinary Ce^{3+} emissions. From Equation 7, the faster decay time of anomalous emission in bromoelpasolites than in chloride compounds can be related to the larger refractive index in bromide than in chloride compounds.

The Stokes shift (ΔS_{an}) relates to the energy difference between the $5d_{e1}$ and the anomalous states. The Stokes shift decreases towards the larger anion. It means that the $5d_{e1}$ which is inside in the conduction band gets closer to the bottom of the conduction band. All Stokes shifts are larger than those of the ordinary Ce^{3+} emission, see column 8 in Table IV.

We could not find a relationship between the Stokes shift and the thermal activation energy (ΔE_q). ΔE_q of $Cs_2NaLuBr_6$: Ce^{3+} is the smallest among the investigated elpasolites. This causes a lower quenching temperature ($T_{0.5}$) in $Cs_2NaLuBr_6$: Ce^{3+} (80 K) than those of Cs_2LiYCl_6: Ce^{3+} (180 K) and $Cs_2LiLuCl_6$: Ce^{3+} (300 K). The attempt rates (Γ_0) for all elpasolites are in the order of 10^{12}-10^{14} Hz.

V. CONCLUSION

$Cs_2NaREBr_6$: Ce^{3+} (RE=La,Y,Lu) are new bromoelpasolites scintillators. $Cs_2NaLaBr_6$: Ce^{3+} emits under X-ray and γ-ray excitation the highest light yield among these compounds (17,000 photons/MeV), whereas $Cs_2NaLuBr_6$: Ce^{3+} has the lowest light yield (5,800 photons/MeV). Scintillation decay curves of bromoelpasolites show a fast 61 ns component with the presence of slow components. We propose that the scintillation mechanism in

$Cs_2NaREBr_6$: Ce^{3+} (RE=La,Y,Lu) is a binary electron-hole recombination.

Cs_2NaYBr_6: Ce^{3+} and $Cs_2NaLuBr_6$: Ce^{3+} show anomalous emission under $4f \rightarrow 5d_{e1}$ Ce^{3+} excitation. This is the first report on anomalous emission in bromoelpasolites and also the first time that two bands of the anomalous emission are observed. These bands are attributed to the transitions from the anomalous state to the $^2F_{5/2}$ and $^2F_{7/2}$ states of Ce^{3+}.

VI. ACKNOWLEDGEMENT

This work was supported by the Dutch Technology Foundation (STW), the Swiss National Science Foundation and the European Community Research Infrastructure Action under the FP6 "Structuring the European Research Area" Programme (through the Integrated Infrastructure Initiative "Integrating Activity on Synchrotron and Free Electron Laser Science"). The authors acknowledge G. Stroganyuk for his assistance in the SUPERLUMI experiments at the HASYLAB of DESY, Hamburg.

[1] B. F. Aull and H. P. Jenssen, Phys. Rev. B **34** 6647 (1986).

[2] T. Pawlik and J. M. Spaeth, Proc. Int. Conf. on Inorganic Scintillators and Their Applications, SCINT95, ed. P. Dorenbos and C. W. E. van Eijk, (Delft University Press, The Netherlands, 1996), p. 392.

[3] C. M. Combes, P. Dorenbos, C. W. E. van Eijk, K. W. Krämer and H. U. Güdel, J. Lumin. **82** 299 (1999).

[4] E. V. D. van Loef, P. Dorenbos, C. W. E. van Eijk, K. W. Krämer and H. U. Güdel, J. Phys.: Condens. Matter **14** 8481 (2002).

[5] C. W. E. van Eijk, A. Bessiere and P. Dorenbos, Nucl. Inst. Meth. Phys. Res. A **529** 260 (2004).

[6] E. V. D. van Loef, P. Dorenbos and C. W. E. van Eijk, K. W. Krämer, H. U. Güdel, Appl. Phys. Lett. **79** 1573 (2001).

[7] A. N. Mishkin, P. A. Rodnyi, A. V. Sidorenko, A. S. Voloshinovskii and P. Dorenbos, Proc. SPIE **47** 4348 (2001).

[8] J. C. van't Spijker, P. Dorenbos, C. W. E. van Eijk, M. S. Wickleder, H. U. Güdel and P. A. Rodnyi, J. Lumin. **72** 786 (1997).

[9] P. Dorenbos, E. V. D. van Loef, C. W. E. van Eijk, K. W. Krämer and H. U. Güdel, Phys. Rev. B **68** 125108 (2003).

[10] A. Bessiere, P. Dorenbos, C. W. E. van Eijk, K. W. Krämer and H. U. Güdel, J. Phys.: Condens. Matter **16** 1887 (2004).

[11] A. Bessiere, P. Dorenbos, C. W. E. van Eijk, K. W. Krämer and H. U. Güdel, A. Galtayries, J. Lumin. **117** 187 (2006).

[12] G. Meyer, Prog. Solid St. Chem. **14** 141 (1982).

[13] G. Zimmerer, Nucl. Instr. Meth. Phys. Res. A **308** 178 (1991).

[14] J. T. M. de Haas, P. Dorenbos and C. W. E. van Eijk, Nucl. Instr. Meth. Phys. Res. A **537** 97 (2005).

[15] W. W. Moses, Nucl. Instr. Meth. Phys. Res. A **336** 253 (1993).

[16] P. Dorenbos, J. T. M. de Haas, R. Visser, C. W. E van Eijk and R. W. Hollander, IEEE Trans. Nucl. Sci. **40** (4) 424 (1993).

[17] Li-Ji. Lyu and D. S. Hamilton, J. Lumin. **48-49** 251 (1991).

[18] R. D. Shannon, Acta Crys. A **32** 751 (1976).

[19] P. Dorenbos, Phys. Rev. B **62** 15640 (2000).

[20] P. Dorenbos, J. Alloys Compounds **341** 156 (2002).

[21] P. Dorenbos, Phys. Rev. B **64** 125117-1 (2001).

[22] P. Dorenbos, Phys. Rev. B **62** 15650 (2000).

[23] Z. Barandiarán, N. M. Edelstein, B. Ordejón, F. Ruipérez and L. Seijo, J. Sol. State Chem. **178** 464 (2005).

[24] P. Dorenbos, Phys. Stat. Sol. A **202** 195 (2005)

[25] E. V. D. van Loef, P. Dorenbos, C. W. E. van Eijk, K. W. Krämer and H. U. Güdel, IEEE Trans. Nucl, Sci. **48** 341 (2002).

[26] T. Tokizaki, T. Makimura, H. Akiyama, A. Nakamura and K. Itoh, Phys. Rev. Lett. **67** 2701 (1991).

[27] B. Henderson and G. F. Imbusch, Optical Spectroscopy of Inorganic Solids, (Clarendon Press, Oxford, 1989).

[28] O. S. Wenger and H. U. Güdel, J. Chem. Phys. **114** 5832 (2001).

Tables

TABLE I: Light yield and energy resolution derived from pulse height spectra of $Cs_2NaLaBr_6$: 0.5% Ce^{3+}, Cs_2NaYBr_6: 0.3% Ce^{3+} and $Cs_2NaLuBr_6$: 0.5% Ce^{3+} under 662 keV γ-ray excitation measured with a Hamamatsu R1791 PMT. Energy resolution was recorded with a shaping time of 10 μs at the 662 keV photopeak.

Compound	Light yield (10^3 photons/MeV)			Energy Resolution
	0.5 μs	3 μs	10 μs	R (%)
$Cs_2NaLaBr_6$: Ce^{3+}	9.0 ± 0.9	14.0 ± 1.4	17.0 ± 1.7	11.3 ± 1.1
Cs_2NaYBr_6: Ce^{3+}	5.0 ± 0.5	6.8 ± 0.7	9.5 ± 1.0	6.3 ± 0.6
$Cs_2NaLuBr_6$: Ce^{3+}	5.2 ± 0.5	5.6 ± 0.6	5.8 ± 0.6	10.5 ± 1.1

TABLE II: Characteristics of the scintillation decay curves and intrinsic decay times of Ce^{3+} of $Cs_2NaLaBr_6$: 0.5% Ce^{3+}, Cs_2NaYBr_6: 0.3% Ce^{3+} and $Cs_2NaLuBr_6$: 0.5% Ce^{3+} at RT. Intrinsic decay times of Ce^{3+} were recorded at 10 K and RT.

Compound	Decay components (relative contribution to total light yield)			Intrinsic Ce^{3+} decay times 10 K / RT
	fast (ns)	intermediate (ns)	slow (μs)	(ns)
$Cs_2NaLaBr_6$: Ce^{3+}	61 ± 6 (32%)	450 ± 50 (11%)	1.9 ± 0.2 (57%)	24 / 30
Cs_2NaYBr_6: Ce^{3+}	61 ± 6 (26%)	350 ± 40 (23%)	2.7 ± 0.3 (51%)	24 / 30
$Cs_2NaLuBr_6$: Ce^{3+}	61 ± 6 (65%)	350 ± 40 (35%)	(Not Observed)	24 / 30

TABLE III: Host properties of $Cs_2NaLaBr_6$, Cs_2NaYBr_6, and $Cs_2NaLuBr_6$. Energies are given in eV.

Compound	E^{fa} (eV)	E^{ex} (eV)	E_{VC} (eV)
$Cs_2NaLaBr_6$	5.71	5.95	6.43
Cs_2NaYBr_6	5.88	6.16	6.70
$Cs_2NaLuBr_6$	6.21	6.46	6.85

TABLE IV: Spectroscopic and crystallographic properties of Ce^{3+} -doped $Cs_2NaREBr_6$ (RE=La,Y,Lu) at RT. ($N : R_{avg}$) represents the anion coordination number and the average distance to the anion (pm). The polyhedron (poly) at the Ce^{3+} site is a *trigonal antiprism* (tap) or *octahedron* (octa). ϵ_c and ϵ_{cfs} are the centroid shift and the crystal field splitting, respectively. λ_{em} and ΔS_{or} are the 5d$\rightarrow^2 F_{5/2}$ emission wavelength and the Stokes shift, respectively. Values between brackets are estimated values.

Compounds	($N : R_{avg}$)	(poly)	5d-excitation bands (nm)	ϵ_c (cm^{-1})	ϵ_{cfs} (cm^{-1})	λ_{em} (nm)	ΔS_{or} (eV)
$Cs_2NaLaBr_6$: Ce^{3+}	(6:285)	(tap)	2x(238), 333, 347, 367	(17200)	(14770)	382	0.13
Cs_2NaYBr_6: Ce^{3+}	(6:276)	(octa)	230, 235, 336, 352, 372	17010	16600	385	0.11
$Cs_2NaLuBr_6$: Ce^{3+}	(6:273)	(octa)	225, 233, 338, 351, 373	16780	17780	389	0.14

TABLE V: Widths of the Ce^{3+} emission bands in chloride and bromoelpasolites (FWHM). Values are derived from the emission spectra recorded at 10 K.

Compounds	Widths of the Ce^{3+} emission bands (eV)				Ref.
	Ordinary Ce^{3+} emission		Anomalous Ce^{3+} emission		
	$^2F_{5/2}$	$^2F_{7/2}$	$^2F_{5/2}$	$^2F_{7/2}$	
Cs_2LiYCl_6: Ce^{3+}	0.338	0.489	-	-	[10]
$Cs_2LiLuCl_6$: Ce^{3+}	0.339	0.480	-	-	[11]
Cs_2NaYBr_6: Ce^{3+}	0.252	0.240	0.346	0.460	This work
$Cs_2NaLuBr_6$: Ce^{3+}	0.273	0.261	0.361	0.485	This work

TABLE VI: The decay times (ns) and decay rates (10^9 Hz) from experiment and modelling curves of $Cs_2NaLuBr_6$: Ce^{3+}. τ_d is the decay time of the $5d_t$ state, τ_a^{tot} and $1/\Gamma_t$ are the decay time for anomalous emission and the transfer rate calculated with Equation 1, data in column 5 and 6 are from fits of Equation 6 to the $5d_t \rightarrow$4f decay curves of Ce^{3+} excited in the $5d_{e1}$ state. $N_a(0)/N_d(0)$ is the ratio in initial populations of the anomalous and $5d_t$ states.

T(K)	τ_d	τ_a^{tot}	$1/\Gamma_t$	$1/(\Gamma_a+\Gamma_t)$	$N_a(0)\Gamma_t/N_d(0)$	$N_a(0)/N_d(0)$
10	24.0	7.83	5.64E35	27.70	0.011	Maximum
30	24.5	7.83	3.81E9	15.13	0.014	5.32E7
60	24.6	7.77	1091	6.75	0.040	44.34
90	24.9	3.75	7.19	3.57	0.180	1.29
110	25.3	1.01	1.16	1.00	0.087	0.101

TABLE VII: Anomalous emission properties; decay time (τ_a), average emission wavelength ($\overline{\lambda}_{an}$), Stokes shift (ΔS_{an}), ratio between the decay time and the average emission wavelength of the anomalous and ordinary Ce^{3+} emissions ($\frac{\tau_a}{(\overline{\lambda}_{an})^3}/\frac{\tau_{or}}{(\overline{\lambda}_{or})^3}$), thermal activation energy (ΔE_q), quenching temperature at which the anomalous Ce^{3+} emission intensity has dropped to 50% of the low temperature value ($T_{0.5}$) and attempt rate (Γ_0) in all studied elpasolites. Values for $\overline{\lambda}_{an}$ and ΔS_{an} are derived from the excitation and emission spectra recorded at 10 K.

Compounds	τ_a (ns)	$\overline{\lambda}_{an}$ (nm)	ΔS_{an} (eV)	$\frac{\tau_a}{(\overline{\lambda}_{an})^3}/\frac{\tau_{or}}{(\overline{\lambda}_{or})^3}$	ΔE_q (eV)	$T_{0.5}$ (K)	Γ_0 (Hz)	Ref.
Cs_3LuCl_6: Ce^{3+}	10.50	281	1.40	0.98	-	80	-	[9]
Cs_2LiYCl_6: Ce^{3+}	9.80	270	1.07	0.99	0.14	180	$5.80.10^{11}$	[10]
$Cs_2LiLuCl_6$: Ce^{3+}	9.40	267	0.99	0.98	0.36	300	$9.02.10^{13}$	[11]
Cs_2NaYBr_6: Ce^{3+}	7.74	273	0.81	0.89	-	-	-	This work
$Cs_2NaLuBr_6$: Ce^{3+}	7.83	273	0.81	0.91	0.08	80	$3.21.10^{12}$	This work

Figure Captions

FIG. 1: X-ray excited emission spectra at RT of (a) $Cs_2NaLaBr_6$: 0.5% Ce^{3+}, (b) Cs_2NaYBr_6: 0.3% $Ce^{3+}$and (c) $Cs_2NaLuBr_6$: 0.5% Ce^{3+}. The dotted lines indicate the peak maxima of the $5d^1 \rightarrow 4f^1 {}^2F_{5/2}$ and $5d^1 \rightarrow 4f^1 {}^2F_{7/2}$ Ce^{3+} emissions.

FIG. 2: Pulse height spectra under ^{137}Cs 662 keV γ-ray excitation of (a) $Cs_2NaLaBr_6$: 0.5% Ce^{3+}, (b) Cs_2NaYBr_6: 0.3% $Ce^{3+}$and (c) $Cs_2NaLuBr_6$: 0.5% Ce^{3+} recorded with a Hamamatsu R1791 PMT and a shaping time of 10 μs. The spectra are stacked for clarity.

FIG. 3: Scintillation decay curves under ^{137}Cs 662 keV γ-ray excitation recorded at RT and Ce^{3+} decay curves excited in the $5d_t$ state recorded at 10 K and RT (inset) of (a) $Cs_2NaLaBr_6$: 0.5% Ce^{3+}, (b) Cs_2NaYBr_6: 0.3% Ce^{3+}, and (c) $Cs_2NaLuBr_6$: 0.5% Ce^{3+}in a semi logarithmic representation. The spectra are stacked for clarity. The solid lines drawn through the data are summed exponential fits.

FIG. 4: Emission spectra of (a) $Cs_2NaLaBr_6$: 0.5% Ce^{3+} excited at 209 (i) and 230 nm (ii), (b) Cs_2NaYBr_6: 0.3% Ce^{3+} excited at 200 (i) and 225 nm (ii) and (c) $Cs_2NaLuBr_6$: 0.5% Ce^{3+} excited at 190 (i) and 222 nm (ii). All spectra were recorded at 10 K.

FIG. 5: Excitation spectra of (a) $Cs_2NaLaBr_6$: 0.5% Ce^{3+} monitoring 407 (i), 360 (ii), and 384 nm (iii) emissions, (b) Cs_2NaYBr_6: 0.3% Ce^{3+} monitoring 390 (i), 345 (ii), and 282 nm (iii) emissions, and (c) $Cs_2NaLuBr_6$: 0.5% Ce^{3+} monitoring 390 (i), 325 (ii), and 285 nm (iii) emissions. The integral spectra (full lines) were recorded at RT, whereas slow (dotted lines) and fast spectra (broken lines) were recorded at 10 K.

FIG. 6: Temperature dependent emission spectra of $Cs_2NaLuBr_6$: Ce^{3+} excited via the 4f→$5d_{e1}$ Ce^{3+} band at 226 nm (a) and integrated intensities of the emission bands (b). Solid curves in (b) are drawn to guide the eye.

FIG. 7: Semi logarithmic plot of the decay time curves of the 282 nm anomalous emission of $Cs_2NaLuBr_6$: Ce^{3+} excited via the 4f→$5d_{e1}$ band (a) and the decay time of the anomalous emission as function of temperature (b). The dotted line through the data is from a model calculation.

FIG. 8: Temperature dependence of the decay curves of the 385 nm $5d_t$ →4f emission of Ce^{3+} in $Cs_2NaLuBr_6$: Ce^{3+} excited into 4f→$5d_e$ band at 226 nm and plotted on a linear scale. The decay time τ_d of the 380 nm $5d_t$ →4f Ce^{3+} emission excited at 333 nm is shown in the inset as function of temperature.

FIG. 9: Crystal field splitting of Ce^{3+} as function of the average distance to neighboring anions in the relaxed lattice. Data on the other elpasolites were added from [22].

FIG. 10: Energy level scheme of $Cs_2NaLuBr_6$: Ce^{3+} and a configuration coordinate diagram illustrating the mechanism for the anomalous emission. The transitions indicated by the numbered arrows are explained in the text.

FIG. 11: Decay curves of 380-385 nm $5d_t$ →4f emission in $Cs_2NaLuBr_6$: Ce^{3+} excited directly in the $5d_t$ state (curves 1) and in the 4f→$5d_{e1}$ state (curves 2) at 60, 90, and 110 K. The solid lines through the data represent the model curves. Parameter values are shown in Table VI

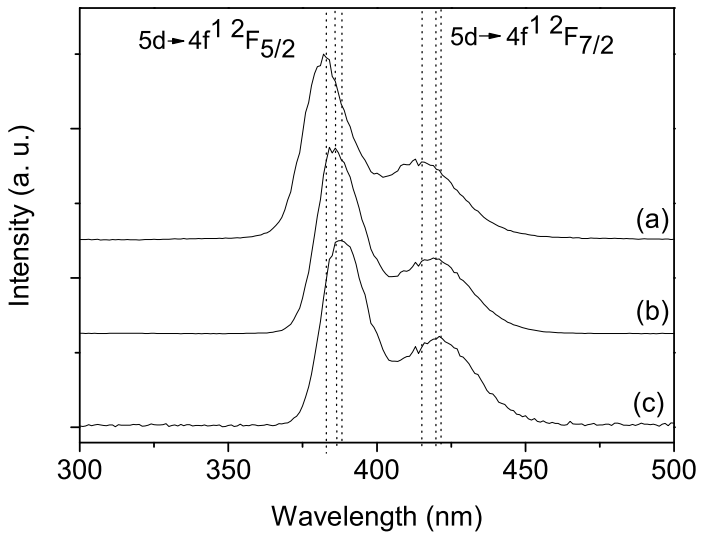
5d→4f1 2F5/2
5d→4f1 2F7/2
Intensity (a. u.)
(a)
(b)
(c)
300
350
400
450
500
Wavelength (nm)

Figure 1

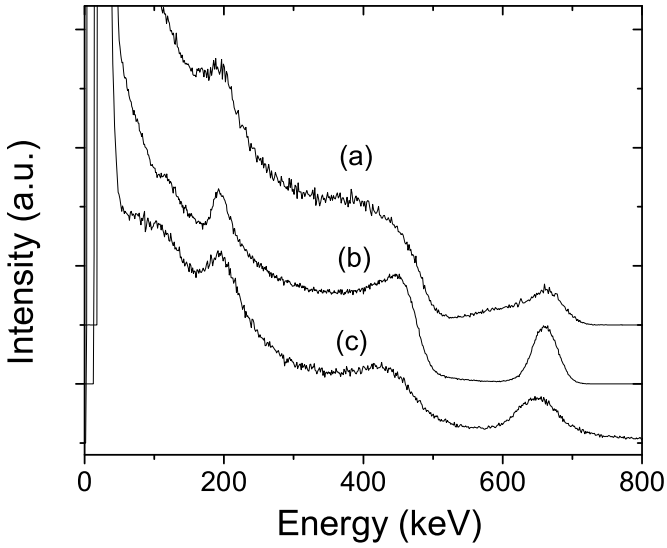

Figure 2

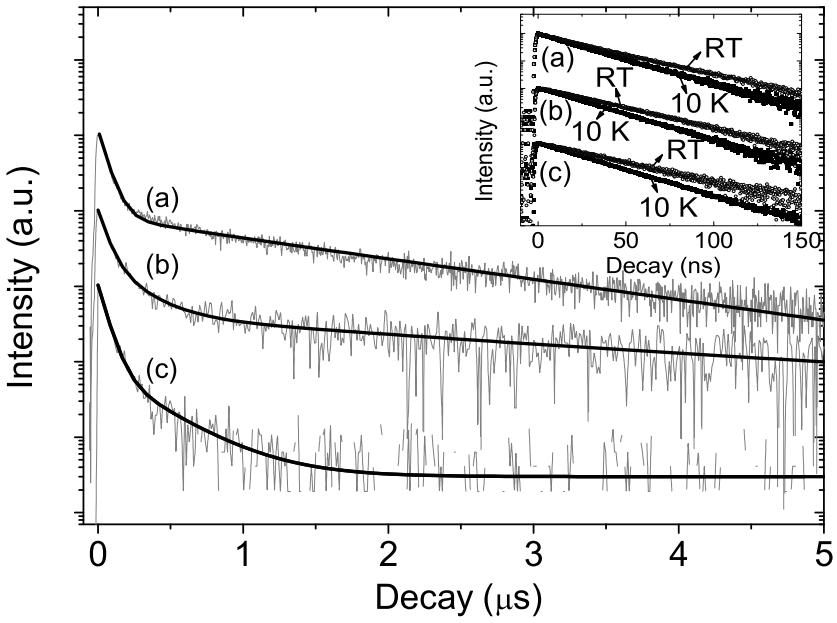
Intensity (a.u.)
(a)
(b)
(c)
0
1
2
3
4
5
Decay (μs)
Intensity (a.u.)
(a)
RT
RT
10 K
(b)
10 K
RT
(c)
10 K
0
50
100
150
Decay (ns)

Figure 3

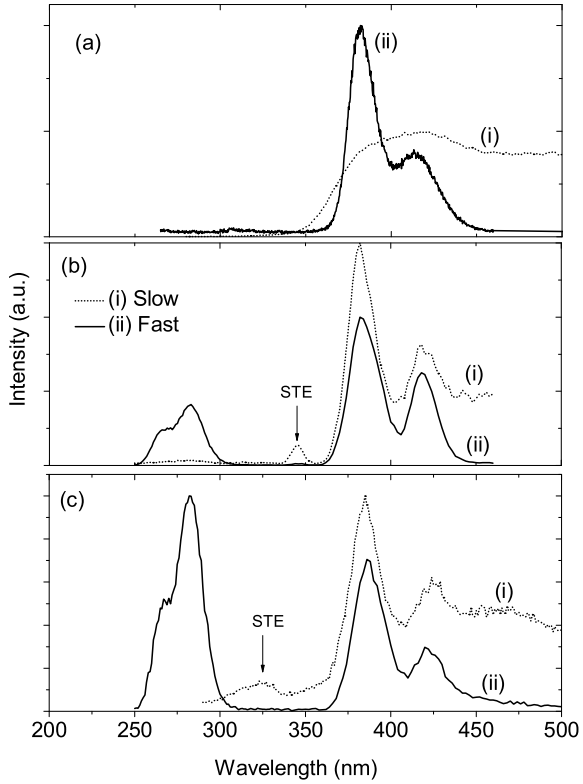
(a)
(ii)
(i)
(b)
(i) Slow
(ii) Fast
STE
(i)
(ii)
(c)
STE
(i)
(ii)
Intensity (a.u.)
200
250
300
350
400
450
500
Wavelength (nm)

Figure 4

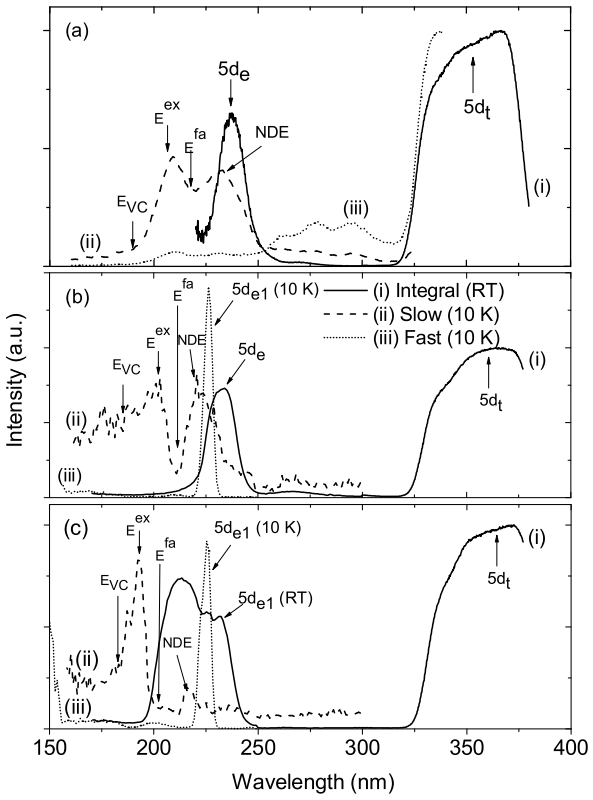
(a)
5d_e
E^ex
E^fa
NDE
E_VC
(ii)
(iii)
5d_t
(i)
(b)
E^fa
5d_e1 (10 K)
(i) Integral (RT)
(ii) Slow (10 K)
(iii) Fast (10 K)
E^ex
NDE
5d_e
E_VC
(ii)
(iii)
5d_t
(i)
(c)
E^ex
E^fa
5d_e1 (10 K)
(i)
E_VC
5d_t
5d_e1 (RT)
NDE
(ii)
(iii)
Intensity (a.u.)
150
200
250
300
350
400
Wavelength (nm)

Figure 5

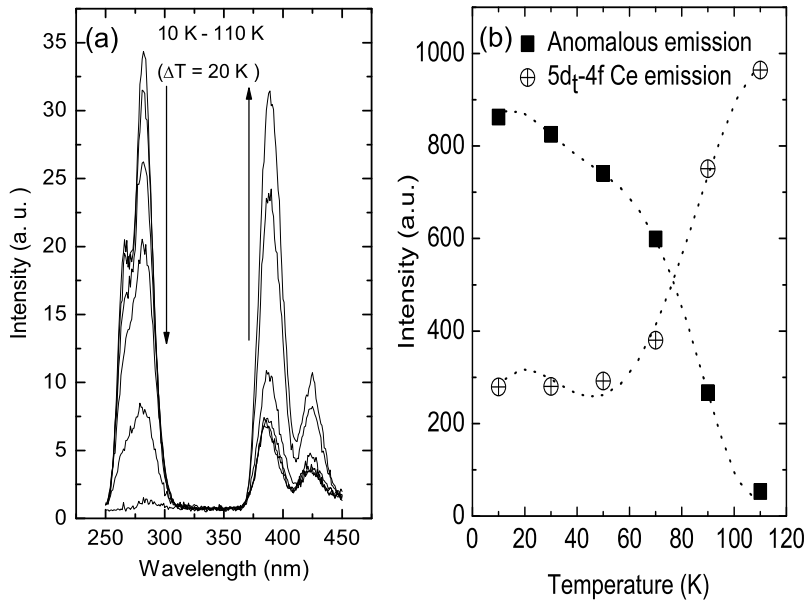
(a)
10 K - 110 K
(ΔT = 20 K)
Intensity (a. u.)
Wavelength (nm)
(b)
Anomalous emission
5d$_t$-4f Ce emission
Intensity (a.u.)
Temperature (K)

Figure 6

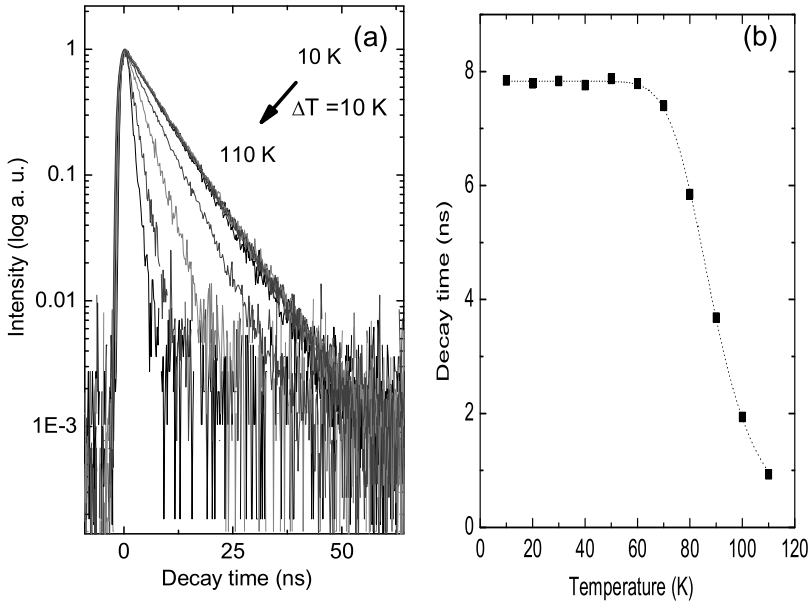
(a)
10 K
ΔT =10 K
110 K
Intensity (log a. u.)
1
0.1
0.01
1E-3
0
25
50
Decay time (ns)
(b)
Decay time (ns)
8
6
4
2
0
0
20
40
60
80
100
120
Temperature (K)

Figure 7

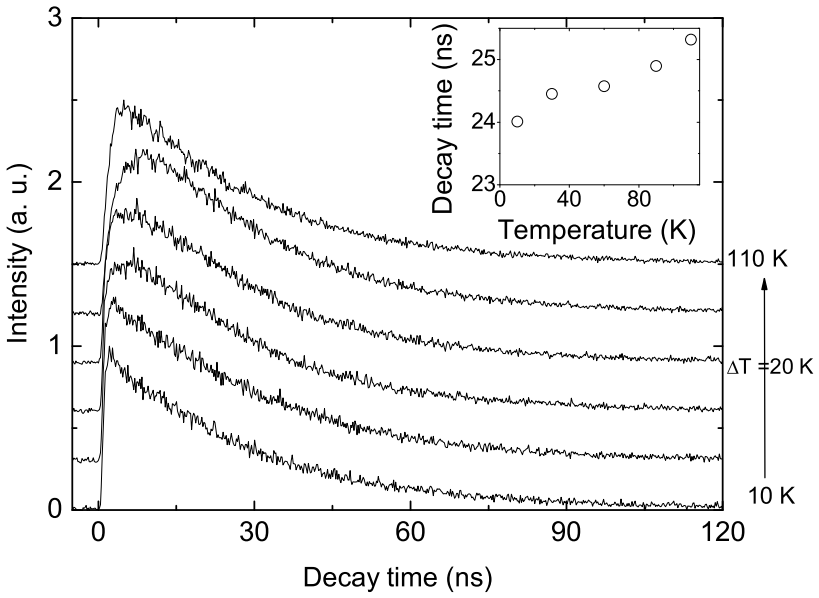
Intensity (a. u.)
Decay time (ns)
Decay time (ns)
Temperature (K)
110 K
ΔT =20 K
10 K

Figure 8

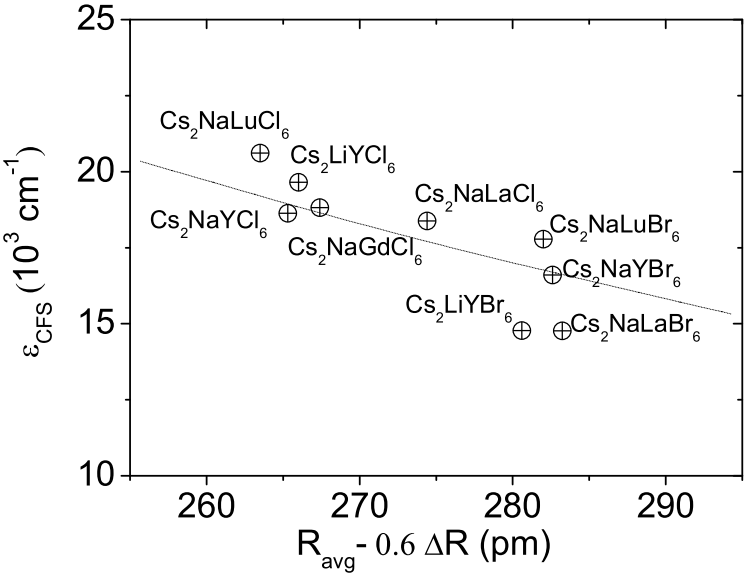
25
20
15
10
260
270
280
290
ε_{CFS} (10^3 cm^{-1})
R_{avg} - 0.6 ΔR (pm)
$Cs_2NaLuCl_6$
Cs_2LiYCl_6
$Cs_2NaLaCl_6$
Cs_2NaYCl_6
$Cs_2NaLuBr_6$
$Cs_2NaGdCl_6$
Cs_2NaYBr_6
Cs_2LiYBr_6
$Cs_2NaLaBr_6$

Figure 9

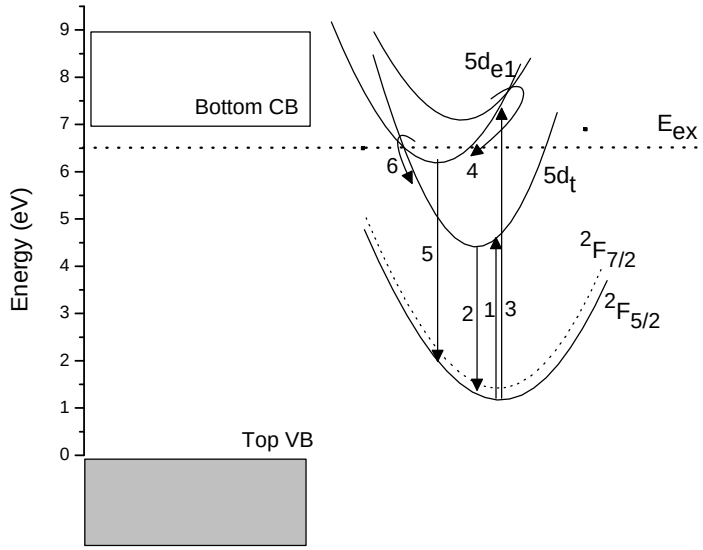
Energy (eV)
9
8
7
6
5
4
3
2
1
0
Bottom CB
Top VB
5d$_{e1}$
E$_{ex}$
5d$_t$
^{2}F$_{7/2}$
^{2}F$_{5/2}$
6
4
5
2
1
3

Figure 10

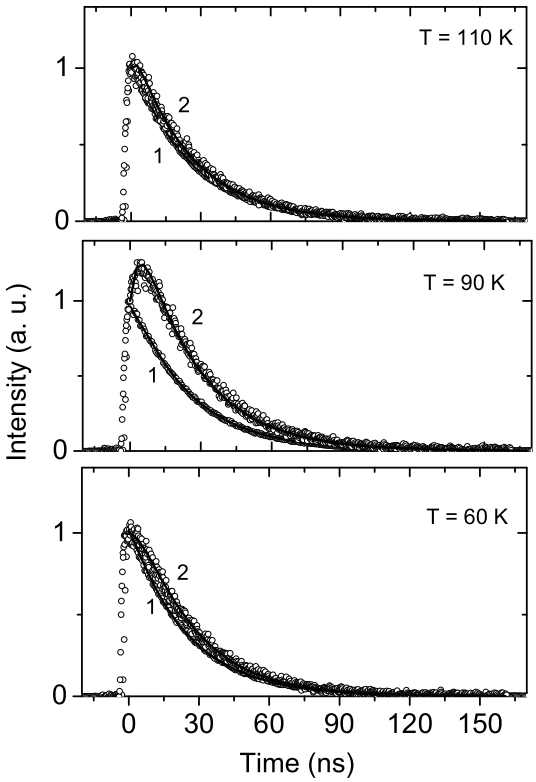

Figure 11